Bulletin of Mathematical Biology (2023) 85:93
https://doi.org/10.1007/s11538-023-01201-z

Society for Mathematical Biology

ORIGINAL ARTICLE

Modeling the Role of Immune Cell Conversion in the Tumor-Immune Microenvironment

Alexander S. Moffett[1,2] · **Youyuan Deng**[3,4] · **Herbert Levine**[1,2,5]

Received: 22 March 2023 / Accepted: 17 August 2023 / Published online: 1 September 2023

Abstract

Tumors develop in a complex physical, biochemical, and cellular milieu, referred to as the tumor microenvironment. Of special interest is the set of immune cells that reciprocally interact with the tumor, the tumor-immune microenvironment (TIME). The diversity of cell types and cell–cell interactions in the TIME has led researchers to apply concepts from ecology to describe the dynamics. However, while tumor cells are known to induce immune cells to switch from anti-tumor to pro-tumor phenotypes, this type of ecological interaction has been largely overlooked. To address this gap in cancer modeling, we develop a minimal, ecological model of the TIME with immune cell conversion, to highlight this important interaction and explore its consequences. A key finding is that immune conversion increases the range of parameters supporting a co-existence phase in which the immune system and the tumor reach a stalemate. Our results suggest that further investigation of the consequences of immune cell conversion, using detailed, data-driven models, will be critical for greater understanding of TIME dynamics.

Keywords Tumor-immune microenvironment · Immune cell conversion · Generalized Lotka-Volterra equations

✉ Herbert Levine
h.levine@northeastern.edu

Alexander S. Moffett
a.moffett@northeastern.edu

Youyuan Deng
youyuan.deng@rice.edu

1 Center for Theoretical Biological Physics, Northeastern University, Boston, MA 02115, USA

2 Department of Physics, Northeastern University, Boston, MA 02115, USA

3 Center for Theoretical Biological Physics, Rice University, Houston, TX 77005, USA

4 Applied Physics Graduate Program, Smalley-Curl Institute, Rice University, Houston, TX 77005, USA

5 Department of Bioengineering, Northeastern University, Boston, MA 02115, USA

1 Introduction

Cancer is a class of evolving diseases, similar in many ways to infectious diseases characterized by viral, bacterial, or eukaryotic parasite infection. Tumor cells can be thought of as cheaters in the cooperative multicellular state from which they are derived, although tumor cells often act collectively in a proto-multicellular manner (Ben-Jacob et al. 2012; Aktipis et al. 2015). The key point is that cancer cells overcome controls ensuring intercellular cooperation and develop into a distinct population upon which evolutionary forces act, not unlike a population of pathogens within a host organism. While this evolutionary nature of cancer has long been acknowledged (Nowell 1976), recent work has rapidly developed our understanding of cancer population dynamics by applying concepts and theoretical tools from evolutionary biology and ecology (Gerlinger et al. 2014; Korolev et al. 2014; Wu et al. 2016; Reynolds et al. 2020). Advances in lineage tracing (Simeonov et al. 2021) and genomics (Navin 2014) technologies have allowed for unprecedented understanding of the complex eco-evolutionary processes underlying tumor growth and metastasis, and theoretical approaches drawing from evolutionary and ecological theory (McFarland et al. 2014; Gluzman et al. 2020; Gatenbee et al. 2022; Kessler and Levine 2022) have enabled predictions of eco-evolutionary phenomena in cancer and interpretation of experimental data. However, much is still unknown about cancer population dynamics, with many complexities still unexplored.

Recent work has developed the concept of the tumor microenvironment (TME), referring to the biochemical, cellular, and physical context in which a tumor exists and how this context impacts tumor behavior (Anderson and Simon 2020). To further emphasize the specific role played by the immune system, one can focus on the tumor-immune microenvironment (TIME). The TIME concept emphasizes that tumors exist in an ecological context of immune and other host cells which influence tumor growth and progression in a complex manner (Binnewies et al. 2018). While there are several clear differences between the ecological interactions of tumors with host cells and traditionally studied interactions in ecology, such as those between predator and prey animals (Kareva et al. 2021), concepts from ecology have nonetheless proved useful in understanding tumor-immune interactions. These concepts hold promise for further untangling the complexities arising from nonlinear, multi-directional interactions between adapting (through varying combinations of mutations and phenotypic plasticity) populations of cells (Hamilton et al. 2022).

While the ability of the immune system to suppress tumor proliferation and metastasis has rightfully received considerable attention (Schreiber et al. 2011), our understanding of how tumors attempt to shape the immune system into cancer-tolerant or even cancer-promoting states remains incomplete (De Visser et al. 2006). While tumors are well-known to affect the metabolic and biochemical state of the TIME (Binnewies et al. 2018; Roy et al. 2021), tumor cells are also able to influence immune cell phenotypes (Flavell et al. 2010), a process known as immune cell conversion. A prime example of immune cell conversion is the polarization of macrophages between M1 and M2 phenotypes (Biswas and Mantovani 2010; Li et al. 2019b). In the M1 phenotype, macrophages produce tumor-suppressing molecules, including nitric oxide and reactive oxygen species, while M2 macrophages produce pro-tumor factors and

promote angiogenesis (Wang et al. 2014; Jetten et al. 2014). Other examples of tumor-influenced immune cell conversion include T cell/regulatory T cell polarization (Liu et al. 2007) and NK cell/ILC1 cell polarization (Gao et al. 2017).

Despite strong evidence for the importance of immune cell conversion in the TIME, this phenomenon has been largely ignored in mathematical models of the TIME. While a number of models exist which include the polarization of immune cells in the TIME (Eftimie and Hamam 2017; Shu et al. 2020), very few (Guo et al. 2023) have included the ability of tumor cells to bias this immune cell polarization. In order to explore the role of immune cell conversion in the TIME, we develop here a minimal mathematical model for tumor-immune interaction including the ability of tumor cells to convert immune cells into a pro-tumor phenotype. Using modified Lotka–Volterra equations, we explore the effects of the rate of immune cell conversion, finding that conversion can be essential to the viability of a tumor population. Specifically, non-zero immune conversion rates can allow for tumor survival in the presence of non-trivial anti-tumor immunity. Our results highlight the need to further inspect the role of tumor-to-immune system feedback, especially in mathematical and computational models of cancer. Furthermore, greater understanding of the consequences of immune cell conversion may have an impact on the development of novel cancer immunotherapies.

2 Model

2.1 Guiding Principles for Tumor-Immune Modeling

Following the work of Wilson and Levy (2012) and Arabameri et al. (2018), we adopt a minimal description of the essential aspects of tumor-immune population dynamics by considering the densities of tumor, anti-tumor immune, and pro-tumor immune cells. This coarse-grained approach greatly simplifies our model and its analysis. This simplification is of course at the expense of the potential quantitative accuracy of a more detailed approach. Once we have established basic mechanisms, future efforts can extend our approach to include a larger number of cell types and more realistic descriptions of interactions.

We proceed by adapting the Lotka-Volterra framework (Wangersky 1978) with multiplicative interaction terms. The resultant ODEs ignore both spatial aspects of tumor-immune interaction and complexities such as saturating interactions. We note that some TIMEs may be better represented by spatially homogeneous models than others. For example, tumor cells in leukemia are largely suspended in the bloodstream, and therefore the assumption that all cells interact with all other cells is a reasonable approximation. For solid tumors, our model assumes that there is no barrier to immune infiltration (Li et al. 2019a). Regardless of which biological scenarios our model is better suited for, we emphasize that our goal is to explore the potential consequences of immune conversion, not to make quantitative predictions about tumor-immune population dynamics.

2.2 A Modified Lotka–Volterra Model

We examine a generalized Lotka–Volterra model describing tumor cell (T), pro-tumor immune cell (P), and anti-tumor immune cell (A) population densities. Our basic innovation is the inclusion of a tumor-induced switching term from anti-tumor to pro-tumor immune phenotypes. We abbreviate pro-tumor immune cells as PTI cells and anti-tumor immune cells as ATI cells. Our baseline model can be written as

$$\frac{dT}{dt} = T\left(r_T - \frac{r_T}{K_T}T + \alpha_{TP}P - \alpha_{TA}A\right) \tag{1}$$

$$\frac{dP}{dt} = P\left(-d_P P + \alpha_{PT}T\right) + \omega AT \tag{2}$$

$$\frac{dA}{dt} = A\left(r_A - \frac{r_A}{K_A}A + \alpha_{AT}T - \alpha_{AP}P\right) - \omega AT, \tag{3}$$

or in condensed vector notation

$$\frac{d\mathbf{N}}{dt} = f(\mathbf{N}),\ \mathbf{N} = \begin{bmatrix} T \\ P \\ A \end{bmatrix}. \tag{4}$$

All parameters are non-negative (Table 1), so that a negative sign in front of a parameter in Eqs. (1)–(3) indicates either inhibition of growth or contribution to death, while a positive sign indicates contribution to growth or inhibition of death. The parameters r_T and r_A describe the "intrinsic" growth rates of tumor and ATI cells each in the absence of other cell types, while K_T and K_A denote their carrying capacities. Quadratic self-limitation terms for tumor and ATI cells are written as r_T/K_T and r_A/K_A for convenience, in a similar manner to previous work (Bunin 2017). By calling r_T and r_A intrinsic growth rates, we mean that they are the growth rates in the absence of other interactions in the model. We assume that PTI cells mostly arise through tumor-induced conversion processes, so we take r_P to be zero, and denote their density-dependent growth inhibition and/or death rate as d_P. The parameters α_{XY} represent the quadratic contributions of interactions between cell types to growth rates, where α_{XY} is the effect of Y on the net growth rate of X. Note that we assumed that contact with tumor cells induces growth of all types of immune cells.

Finally, as mentioned above, we include terms reflecting the ability of tumor cells to induce some immune cells that inhibit tumor growth, such as M1 macrophages, to switch phenotypes into functionally pro-tumor states, such as M2 macrophages. This is reflected in Eqs. (1)–(3) by a conversion parameter $\omega \geq 0$ controlling the rate at which tumor cells induce ATI cells to switch to PTI cells. We assume that all of these parameters are independent of time and cell concentrations.

Table 1 Parameter values used in figures

Parameter	Figure 2	Figure 3	Figure 4	Figure 5	Figure 6	Figure 7
r_T	1	1	1	1	1	1
K_T	1	1	1	1	1	1
d_P	1	1	1	1	1	1
r_A	1	1	1	1	1	1
K_A	1	1	1	1	1	1
α_{TP}	0.95	0.95	0.95	0.95	0.95	0.95
α_{TA}	[0, 2]	[1, 20]	1.5	1.5	[1, 1.5]	1.5
α_{PT}	0.15	0.15	0.15	0 or 0.15	0.15	[0, 1.5]
α_{AT}	0.05	0.05	0.05	0.05	0.05	0.05
α_{AP}	0.5	0.5	0.5	0.5	0.5	0.5
ω	[0, 2]	[0, 2]	[0, 1]	[0, 5]	[0, 0.75]	0.5

$[a, b]$ means that parameters vary in the closed interval from a to b

2.3 Types of Steady States

We refer to states of the system as feasible when the densities of all cell types are non-negative

$$\mathbf{N} \geq 0 \iff T,\ P,\ A \geq 0 \tag{5}$$

corresponding to physically meaningful states of the system. Equations (1)–(3) can support the following types of feasible steady states beyond the trivial steady state $T = P = A = 0$:

(**T**) Tumor-only: $T > 0$ and $P = A = 0$
(**A**) ATI-only: $A > 0$ and $T = P = 0$
(**TA**) Tumor-ATI coexistence: $T, A > 0$ and $P = 0$
(**TP**) Tumor-PTI coexistence: $T, P > 0$ and $A = 0$
(**TPA**) Tumor-PTI-ATI coexistence: $T, P, A > 0$.

Tumor-only (**T**) and ATI-only (**A**) steady states always exist and are always feasible in the allowed parameter space, while the simultaneous feasibility and existence of steady states **TA**, **TP**, and **TPA** depend on the choice of parameters. As we will see, there can be at most one steady state corresponding to types **T**, **A**, **TA**, and **TP**, while there can be more than one tumor-PTI-ATI coexistence (**TPA**) steady state.

We denote the set of steady state solutions corresponding to each type as $\mathcal{S}_X$, where X in the subscript indicates the cell types that are positive in the steady state. For example, for the tumor-only steady states, we have

$$\mathcal{S}_T = \{\mathbf{N} \in \mathbb{R}^3 \mid f(\mathbf{N}) = \mathbf{0},\ T > 0,\ P = A = 0\}, \tag{6}$$

while for tumor-PTI-ATI coexistence steady states we have

$$\mathcal{S}_{TPA} = \{\mathbf{N} \in \mathbb{R}^3 \mid f(\mathbf{N}) = \mathbf{0},\ \mathbf{N} > 0\}. \tag{7}$$

Because there can be at most one feasible steady state for each of the types (**T**), (**A**), (**TA**), and (**TP**), we can unambiguously refer to *the* steady state meeting the respective criteria of these types, writing these as

$$\mathbf{T} \in \mathcal{S}_T,\ \mathbf{A} \in \mathcal{S}_A,\ \mathbf{TA} \in \mathcal{S}_{TA},\ \mathbf{TP} \in \mathcal{S}_{TP}. \tag{8}$$

We can refer to steady states with tumor-PTI-ATI coexistence similarly

$$\mathbf{TPA} \in \mathcal{S}_{TPA}, \tag{9}$$

but we must often take care to specify which solution in $\mathcal{S}_{TPA}$ we are referring to.

2.4 Linear Stability Analysis

In order to assess the linear stability of steady states, we use the Jacobian matrix

$$\nabla f(\mathbf{N}) = \begin{bmatrix} r_T - 2\frac{r_T}{K_T}T + \alpha_{TP}P - \alpha_{TA}A & \alpha_{TP}T & -\alpha_{TA}T \\ \alpha_{PT}P + \omega A & -2d_P P + \alpha_{PT}T & \omega T \\ (\alpha_{AT} - \omega)A & -\alpha_{AP}A & r_A - 2\frac{r_A}{K_A}A + (\alpha_{AT} - \omega)T - \alpha_{AP}P \end{bmatrix}, \tag{10}$$

obtained from taking partial derivatives of the right-hand side of Eqs. (1)–(3) with respect to T, P, and A, and check whether the real parts of its eigenvalues are all negative. When this is the case, the Hartman-Grobman theorem allows us to identify a steady state as stable. When at least one eigenvalue of the Jacobian is positive, the steady state is unstable. When at least one eigenvalue is zero, while all others are negative, we cannot determine whether the steady state is stable from the linearized system alone. In this case, we provide numerical evidence for the asymptotic stability (or instability) of a steady state.

2.5 Computational Methods

We performed all numerical ODE integration and root finding using SciPy 1.7 (Virtanen et al. 2020). We used NumPy 1.21 Harris et al. (2020) in most calculations. For creating plots, we used Matplotlib 3.5 (Hunter 2007) within a Jupyter notebook (Kluyver et al. 2016). We used the scikit-learn 1.0 (Pedregosa et al. 2011) support vector machine implementation with a degree 3 polynomial kernel for visualizing the interfaces between basins of attraction in Fig. 4.

3 Results

3.1 Characterizing the Steady States Through Feedback and Invasion Growth Rates

As described above, we can classify the steady states of our model by the cell types that have non-zero density. For all classes of steady states, except for the case of tumor-PTI-ATI coexistence (**TPA**) with $\omega > 0$, we can write the steady state densities in simple terms of the model parameters (Table 2). We can further simplify these expressions by gathering parameters into terms describing effective growth rates, written as $\Omega_{X\to Y}$, meaning the net growth rate of X when "invading" a steady state population of Y, and net negative feedback, written as $\Gamma_{X\to Y;S}$, meaning the net negative feedback of X on Y at the specified steady state S. For example, the effective growth rate of tumor cells in a population of ATI cells is

$$\Omega_{T\to \mathbf{A}} = r_T - \alpha_{TA} K_A \tag{11}$$

We note that by "invasion" we refer to the general concept of invasive populations in ecological settings, rather than the specific physical movement of one type of cell into a population of another type of cell (although this could constitute an invasion by our definition). Invasive species and their effects on ecosystems are an important topic of study in ecology. In theoretical ecology, invasions have been given a precise definition to serve as a mathematical tool for analyzing the robustness of communities against invasive species. Suppose we catalog $n > 0$ different species and index them by the set $\{1, 2, \ldots, n\}$. Within a community, we observe a steady state, described by the vector of densities of each species within the community, $\mathbf{N}^\star$. Suppose that $N_i^\star > 0$ for at least one species $i \in \{1, 2, \ldots, n\} \setminus \{j\}$, while $N_j^\star = 0$ for some focal species $1 \le j \le n$. An infinitesimal density of species j is then introduced into the community, representing the introduction of an invasive species, whether through natural migration or human intervention. Species j is said to invade the community if the per-capita growth rate of species j is positive, or using our notation described above

$$\Omega_{j\to \mathbf{N}^\star} \equiv \lim_{\delta N_j \to 0^+} \frac{1}{\delta N_j} \frac{dN_j}{dt}\bigg|_{\mathbf{N}=\mathbf{N}^\star+\delta\mathbf{N}} > 0 \tag{12}$$

with the density introduced through invasion defined as

$$\delta N_i = \begin{cases} 0 & i \neq j \\ \delta N_j > 0 & i = j. \end{cases} \tag{13}$$

We use this definition of invasions throughout the article.

As an example of net negative feedback, we define the net negative feedback of tumor cells on tumor cells in the tumor-PTI-ATI coexistence state (**TPA**) with $\omega = 0$

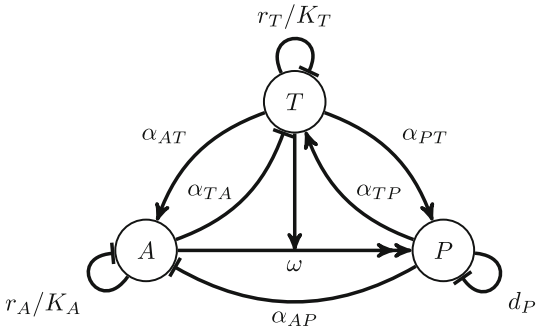

Fig. 1 Schematic diagram of interactions in the model. Note that the exponential growth terms r_T and r_A are not depicted. The meanings of each type of line between T, P, and A are as follows. Single pointed arrow: positive ("activating") interaction; Line with straight, perpendicular end: negative ("inhibiting") interaction; Double pointed arrow with perpendicular, bisecting single pointed arrow: conversion interaction, here conversion of A to P is "catalyzed" by T

as

$$\Gamma_{T\to T;\mathbf{TPA}} = \frac{r_T}{K_T} + \frac{\alpha_{TA}\alpha_{AT}}{r_A/K_A} - \frac{\alpha_{TA}\alpha_{AP}\alpha_{PT}}{(r_A/K_A)d_P} - \frac{\alpha_{TP}\alpha_{PT}}{d_P}. \tag{14}$$

This quantity arises from rearrangement of the **TPA** the steady state solution of Eqs. (1)–(3) with $\omega = 0$, and adds up all the contributions to tumor negative self-feedback, which can be visualized in Fig. 1. The first term, r_T/K_T, is direct tumor self-limitation. The second term reflects the positive effect of tumor density of ATI cell growth, which in turn inhibits tumor growth. This effect is mitigated by strong ATI self-limitation, which is why r_A/K_A appears in the denominator. The third and fourth terms are actually positive feedback, and hence have negative signs in the net *negative* feedback, $\Gamma_{T\to T;\mathbf{TPA}}$. The third term represents the positive effect that tumor cell density has on PTI cell growth, while PTI cell density has a negative effect on ATI cell growth, and ATI cell density has a negative effect on tumor cell growth. Thus, tumor cell density activates PTI cell growth which inhibits the growth of tumor-inhibiting ATI cells, a net positive effect on tumor growth. Finally, the fourth term represents tumor cell density activating PTI cell growth, which then activates tumor cell growth. Self limitation terms also appear in the denominators of the third and fourth terms, for the same reasons as discussed for the second term.

Note that the feedback $\Gamma_{X\to Y;S}$ depends directly on the state S, because zero density of one or more cell types will remove feedback "channels", limiting the number of ways that feedback can be felt by a cell type. To illustrate this, we can compare the net feedback of tumor cells on tumor cells in the tumor-PTI-ATI coexistence state (Eq. 14) with that for the tumor-PTI coexistence state (**TP**)

$$\Gamma_{T\to T;\mathbf{TP}} = \frac{r_T}{K_T} - \frac{\alpha_{TP}\alpha_{PT}}{d_P} \tag{15}$$

which lacks all interaction parameters with ATI cells (see Fig. 1).

Table 2 Summary of steady states

	T	**A**	**TA**
T	K_T	0	$K_T\left(1-\frac{\alpha_{TA}}{r_T}\frac{\Omega_{A\to\mathbf{T}}}{\Gamma_{A\to A;\mathbf{TA}}}\right)$
P	0	0	0
A	0	K_A	$\frac{\Omega_{A\to\mathbf{T}}}{\Gamma_{A\to A;\mathbf{TA}}}$
Feasible	Always	Always	$r_T-\alpha_{TA}\frac{\Omega_{A\to\mathbf{T}}}{\Gamma_{A\to A;\mathbf{TA}}}>0$
Stable	Never	$\Omega_{T\to\mathbf{A}}<0$	Never
States	1	1	0 (if $\omega\neq 0$) or 1

	TP	**TPA** ($\omega=0$)	**TPA** ($\omega>0$)
T	$\frac{r_T}{\Gamma_{T\to T;\mathbf{TP}}}$	$\frac{\Omega_{T\to\mathbf{A}}}{\Gamma_{T\to T;\mathbf{TPA}}}$	See Appendix A
P	$\frac{\alpha_{PT}}{d_P}\frac{r_T}{\Gamma_{T\to T;\mathbf{TP}}}$	$\frac{\alpha_{PT}}{d_P}\frac{\Omega_{T\to\mathbf{A}}}{\Gamma_{T\to T;\mathbf{TPA}}}$	See Appendix A
A	0	$K_A-\frac{\Gamma_{T\to A;\mathbf{TPA}}}{r_A/K_A}\frac{\Omega_{T\to\mathbf{A}}}{\Gamma_{T\to T;\mathbf{TPA}}}$	See Appendix A
Feasible	$\frac{r_T}{K_T}>\frac{\alpha_{TP}\alpha_{PT}}{d_P}$	See Appendix A	See Appendix A
Stable	$\omega>\Gamma_{T\to T;\mathbf{TP}}\frac{r_A}{r_T}+\alpha_{AT}-\frac{\alpha_{AP}\alpha_{PT}}{d_P}$	See Appendix A	See Appendix A
States	1	0 or 1	0 or 1 or 2

See Appendix A for details

The tumor-only (**T**) and tumor-ATI coexistence (**TA**) steady states are always unstable (Table 2), and are therefore of no interest for our purposes. This leaves the ATI-only (**A**), tumor-PTI coexistence (**TP**), and tumor-PTI-ATI coexistence (**TPA**) states as the focus of our analysis. These can be thought of respectively as immune "wins", tumor "wins", and tumor-immune "draw". To narrow the parameter space of interest, we can see that **TP** is feasible only when

$$\frac{r_T}{K_T}>\frac{\alpha_{TP}\alpha_{PT}}{d_P}\text{ or equivalently }\Gamma_{T\to T;\mathbf{TP}}>0 \tag{16}$$

is satisfied. This can be interpreted to mean that the direct negative feedback of tumor cells on themselves must be greater than the positive feedback of tumor cells on themselves through PTI cells, where the feedback signs are clear from Eqs. (1) and (2) (tumors are self-limiting through r_T/K_T while tumor cells increase PTI growth rate and PTI cells increase tumor growth rate). If this condition is violated, unbounded tumor growth is possible (see Fig. 7), contradicting the biophysical realities of cancer. Thus, we can reasonably focus on the parameter space where Eq. (16) is met, as we do throughout the remainder of this work.

3.2 Stability of Steady States

The stability conditions we have derived for several of the steady states have several interesting implications. The **A** state is only stable when the tumor invasion growth

rate ($\Omega_{T\to\mathbf{A}}$) is negative (Table 2). When $\omega = 0$, a necessary condition for the **TPA** state to be stable is that $\Gamma_{T\to T;\mathbf{TPA}} > 0$ (Appendix A). This means that the only way for there to be a feasible, stable tumor-PTI-ATI steady state when $\omega = 0$ is for $\Omega_{T\to\mathbf{A}}$ to be positive (Table 2). Thus, when $\omega = 0$ the **A** and **TPA** steady states cannot both be feasible and stable. There can, however be bistability for $\omega = 0$ between the **A** and **TP** states.

The stability of the **TP** state can switch when ω is increased, provided that the right-hand side of the stability condition

$$\omega > \Gamma_{T\to T;\mathbf{TP}}\frac{r_A}{r_T} + \alpha_{AT} - \frac{\alpha_{AP}\alpha_{PT}}{d_P} \tag{17}$$

is positive. We will see in the next section that this stability switch corresponds to a transcritical bifurcation where the **TPA** state collides with the **TP** state. The **TP** state can only be stable for $\omega = 0$ when the right-hand side of Eq. 17 is negative (see Appendix A). While we can exactly solve for the **TPA** state and the eigenvalues of the corresponding Jacobian for any ω value, the complexity of the resulting expressions prevent clear interpretation. See Appendix A for a more detailed account of solving for **TPA**.

3.3 Viability of Tumor Cell Populations is Dependent on Immune Cell Conversion

Given the stability conditions discussed in the previous section, there are several possible scenarios exhibited by the tumor-immune ecosystem when immune cells cannot be converted ($\omega = 0$). There can be a single, stable, steady state, either **A** or **TPA**, or there can be bistability between **A** and **TP**. This bistability can only occur when ATI cells cannot invade the **TP** state ($\Omega_{A\to\mathbf{TP}} < 0$, see Appendix A and Eq. (52)), an exceptionally hostile environment to ATI cells for a normally functioning immune system. Because $\Omega_{A\to\mathbf{TP}}$ depends only on the model parameters, the choice of parameters for the model in some sense reflect the long-term development of the tumor while the dynamics of the model reflect faster processes. A parameter set where $\Omega_{A\to\mathbf{TP}} < 0$ reflects a decidedly pro-tumor TIME where immune cell conversion is less relevant than when $\Omega_{A\to\mathbf{TP}} > 0$, where ω must be positive for bistability between **A** and **TP** (healthy and cancerous states, respectively).

The behavior is of more interest in this second case, where we consider non-zero ω effects. The top row of Fig. 2 shows the behavior of the steady states as ω varies when $\Omega_{T\to\mathbf{A}} \geq 0$, where an increasing killing rate of tumor cells by ATI cells (α_{TA}) decreases the tumor density in **TPA**. When $\Omega_{T\to\mathbf{A}} = 0$, as shown in the first row of Fig. 2 (darkest green curve in the subplot), the stable **TPA** solution disappears altogether at $\omega = 0$, while the **A** state switches from being unstable to stable. Thus, when $\Omega_{T\to\mathbf{A}}$ is non-negative, there is no stable healthy state (**A**) of the system, while once $\Omega_{T\to\mathbf{A}}$ becomes negative the healthy state becomes stable. When there is no stable state with non-zero tumor cell density at $\omega = 0$ ($\Omega_{T\to\mathbf{A}} < 0$), a saddle node bifurcation occurs at a positive ω (Fig. 2). Above this ω value, there are two **TPA** steady states, one stable and one unstable. As ω increases, eventually the stable **TPA** solution collides with the **TP** state, exchanging stability in a transcritical bifurcation.

For larger ω values, past the transcritical bifurcation, there is bistability between the **A** and **TP** states.

The saddle node bifurcation occurs at larger ω values as α_{TA} increases, meaning that in order to maintain a positive steady state population density, tumor cells must convert ATI cells more rapidly when ATI cells kill tumor cells more efficiently. When α_{TA} is large enough, the stable branch of the **TPA** state disappears and a pitchfork bifurcation occurs at $\omega = \Gamma_{T\to T;\mathbf{TP}}\frac{r_A}{r_T} + \alpha_{AT} - \frac{\alpha_{AP}\alpha_{PT}}{d_P}$ (Fig. 3). For even larger α_{TA} values, the ω value at which the saddle node bifurcation occurs decreases, but the stable **TPA** steady state is no longer feasible.

There are several interesting biological implications of these results. First, we would expect to see a minimal immune cell conversion rate for tumor viability, below which the tumor cannot be sustained. This is visible in the second row of Fig. 2, for ω values below the the saddle node bifurcations. We would not expect to observe this phenomenon in all cases, as we see viable tumor cell populations at $\omega = 0$ for tumor-friendly parameters, as mentioned above. Rather, we would expect to find minimal immune conversion rates for tumor viability in the early stages of tumor development. This is a testable prediction of our model. If the production rate or degradation rate of the biochemical messengers mediating immune cell conversion, such as TGFβ (Flavell et al. 2010) can be experimentally manipulated, it should be possible, albeit perhaps technically difficult, to examine the effects of ω on tumor viability in vitro.

Second, our model suggests that a "stalemate" state (**TPA**) can exist at intermediate immune conversion rates, as seen in all subplots of Fig. 2. The steady state with coexistence between tumor cells, PTI cells, and ATI cells represents a stalemate between pro-tumor and anti-tumor cell types, consistent with previously hypothesized "equilibrium" tumor states (Koebel et al. 2007). In the context of metastasis, this possibility is sometimes referred to as tissue dormancy. We predict that, intuitively, the possible sizes of "equilibrium" tumor populations are limited by the ability of ATI cells to kill tumor cells (α_{TA}, see Fig. 2).

Third, we find that there can be an intermediate immune cell conversion rate at which the tumor population density is maximal in the stable **TPA** state, as can again be seen in all subplots of Fig. 2. This is due to the fact that the steady state ATI cell "reservoir" for producing PTI cells shrinks as ω increases, so that in some parameter sets there is an optimal $\omega_{\max}$ such that for larger $\omega > \omega_{\max}$, the tumor cell density is less than at $\omega_{\max}$. This phenomenon occurs as the stable **TPA** solution approaches the **TP** solution, in which the anti-tumor immune system is non-existent in the local TIME. While it is unclear how well a complete (local) lack of ATI cells reflects a late stage TIME, the possibility of an intermediate immune cell conversion rate that maximizes tumor cell density has not, to our knowledge, been discussed previously.

Finally, our model predicts that above a threshold immune cell conversion rate, large tumor killing rates by ATI cells (α_{TA}) are not sufficient to eradicate stable states with positive tumor density (Fig. 3). In this way, immune cell conversion can protect tumor viability against even an extraordinarily effective immune system.

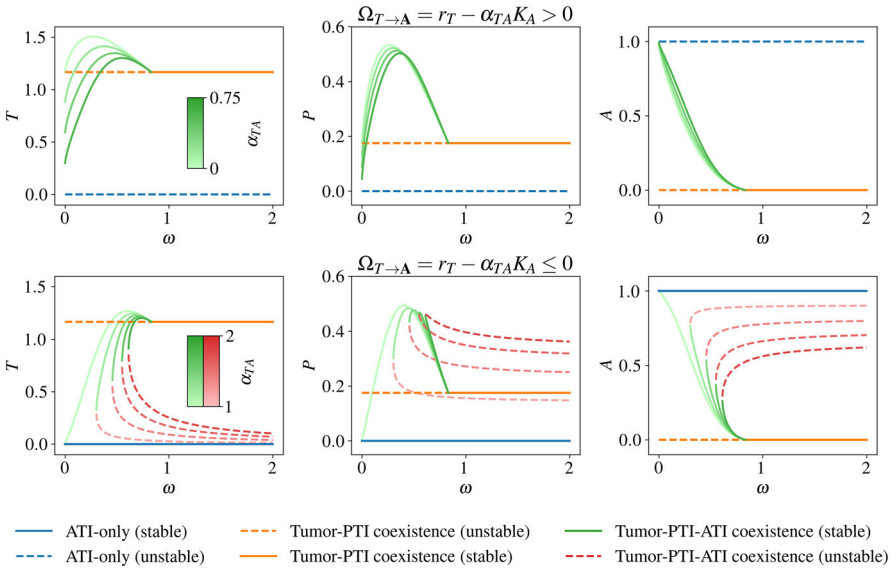

Fig. 2 Bifurcation diagrams over ω for different ATI tumor-killing rates (α_{TA}). When tumor cells can invade an ATI-only state ($\Omega_{T\to\mathbf{A}} > 0$, first row), there is no stable steady state with $T = 0$. When $\Omega_{T\to\mathbf{A}} = 0$ ($\alpha_{TA} = 1$ in the first row, with the **TPA** steady state shown in the darkest shade of green) then the **A** and **TPA** states collide at $\omega = 0$, and as ω increases the **TPA** state changes continuously from the **A** state. The **TPA** state has increasing values of T and P as ω increases, until it collides with the **TP** state in a transcritical bifurcation, swapping stabilities. When tumor cells cannot invade an ATI-only state ($\Omega_{T\to\mathbf{A}} < 0$, second row), there is always a stable cancer-free state **A**. At $\omega = 0$ the only stable steady state is **A**, with the **TPA** steady state appearing for $\omega > 0$; there is a saddle node bifurcation at a value of ω, below which there is no steady state with positive tumor density. Above this value of ω, there is bistability between the cancer-free and cancer states. The first column shows the steady state densities of tumor cells, while the second column shows the density of PTI cells, and the third column shows the density of ATI cells. Only feasible steady states are shown. Note that each individual subplot is a projection onto to T, P, or A densities from the full three-dimensional state space, so that intersections of solutions occur only when curves in all three projections intersect (Color figure online)

3.4 Immune Cell Conversion Promotes Tumor Survival at Small Growth Rate

As discussed in the previous section, our model indicates that when $\Omega_{T\to\mathbf{A}} = r_T - \alpha_{TA}K_A \leq 0$, there cannot be a stable **TPA** state when $\omega = 0$. While we have focused on the effects of α_{TA} in Fig. 2, it is clear that reducing r_T (reflecting a decreased tumor growth rate) or increasing K_A (reflecting a larger ATI cell carrying capacity) can yield similar results. When the intrinsic tumor growth rate (r_T), the rate of ATI cells killing tumor cells (α_{TA}), and the ATI cell carrying capacity (K_A) yield a negative $\Omega_{T\to\mathbf{A}}$, we observe bistability between **A** (cancer-free) and either **TPA** or **TP** (cancer), provided that ω is large enough. This leads to basins of attraction for the cancer-free and cancer states, divided by an ω-dependent two-dimensional surface (Fig. 4).

This bistability between a state with zero tumor density and a state with positive tumor density is an example of an Allee effect, a term commonly used in ecology (Korolev et al. 2014). With an initially low tumor density, the system will evolve towards the cancer-free state, while with sufficiently large tumor and ATI cell density

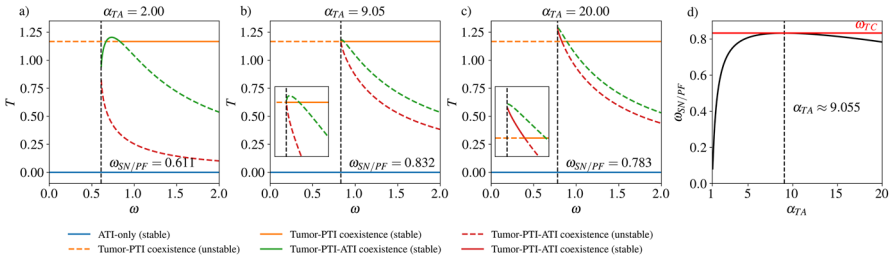

Fig. 3 Values of ω for saddle node and pitchfork bifurcations. (**a**–**c**) Bifurcation diagrams showing the steady state tumor cell density as ω is changed, as in Fig. 2, for three representative α_{TA} values. a) For $\alpha_{TA} = 2$, we see the same behavior as in the last row of Fig. 2. **b** At $\alpha_{TA} \approx 9.05$, there is a pitchfork bifurcation rather than a saddle node bifurcation. The inset subfigure shows a zoomed-in view of the pitchfork bifurcation. **c** For the large value of $\alpha_{TA} = 20$, there is again a saddle node bifurcation, which occurs at a value of ω which now decreases as α_{TA} is further increased. The stable part of the lower red branch of the tumor-PTI-ATI solution (before colliding with the tumor-PTI solution in a transcritical bifurcation) is not feasible. The inset subfigure shows a zoomed-in view of the saddle node and transcritical bifurcations. d) The value of ω at which the saddle node bifurcation (or pitchfork bifurcation in the special case of $\alpha_{TA} \approx 9.055$) occurs, labeled as $\omega_{SN/PF}$, as a function of α_{TA}. The ω value where the tumor-PTI-ATI solution and the tumor-PTI solution collide in a transcritical bifurcation ($\omega_{TC} \approx 0.832$) is shown as a red horizontal line (Color figure online)

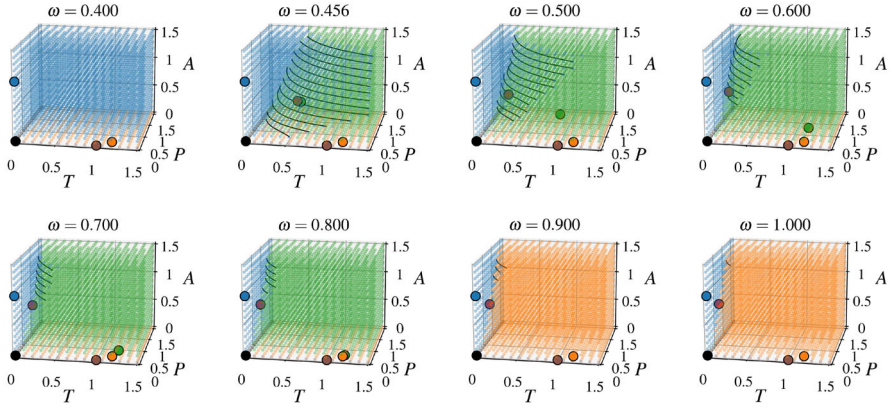

Fig. 4 The basins of attraction with increasing ω. As ω increases, the region of initial states that end up at the cancer-free state diminishes rapidly, while the basins of attraction for states with positive tumor density increase in volume. Each subplot depicts a three-dimensional grid of points representing initial values of T, P, and A. The larger dots with black edges indicate the locations of steady states, with colors matching those in Fig. 2 (note that the $T = P = A = 0$ and **T** steady states, shown in black and brown respectively, are not shown in Fig. 2). The points in the three-dimensional grid are colored according to the steady state that they asymptotically approach in numerical integration of Eqs. (1)–(3). The black curves are estimates of the dividing surface contours separating basins of attraction, found using support vector machines with degree 3 polynomial kernels as implemented in scikit-learn 1.0 (Pedregosa et al. 2011) (Color figure online)

the system will evolve towards the cancer state. As the ATI-to-PTI conversion rate increases, the region of state space where the system will evolve towards the cancer free state shrinks (Fig. 4). This means that if the system is initially in the cancer-free state, the amount of tumor density that must be introduced for the system to reach the cancer state decreases as ω increases. Without any ATI-to-PTI conversion ($\omega = 0$),

there cannot be bistability between the **A** and **TPA** states. However, there can still be bistability between **A** and **TP** with $\omega = 0$ when

$$r_A + \alpha_{AT} T - \alpha_{AP} P \leq 0 \tag{18}$$

where T and P here are the steady state densities in the **TP** state (see discussion on Appendix A and Eqs. (49)–(52) therein). This means that the growth rate of a small ATI density introduced to the **TP** state must be negative, consistent with a developed TIME state that is uninhabitable for ATI cells. Thus, while an ATI-to-PTI conversion term is not strictly necessary for bistability, it allows for bistability in a broader range of parameter sets with biological relevance.

Finally, we note that this baseline model does not exhibit tristability. That is, the existence of a stable **TPA** state means that, for some range of parameters, further growth of the tumor is precluded by an increasing immune response. There is no mechanism whereby even a large increase in tumor size could overcome this linear response, hypothetically giving rise to **A**, **TP**, **TPA** tristability. We cannot exclude the possibility that a more complete model might exhibit such a parameter region.

3.5 Alternate Modeling Choices Yield Similar Results

While we have sought to analyze a minimal model of tumor-immune interaction, there are several alternate modeling choices we could have made, depending on assumptions about the behavior of the immune system. In order to test the effects of changing our assumptions, we consider three modifications to our original model in Eqs. (1)–(3)

1. Linearity of PTI direct self feedback: $-d_P P^2$ or $-d_P P$ in Eq. (2)
2. Direct positive feedback from tumor cells to PTI cells: $\alpha_{PT} > 0$ or $\alpha_{PT} = 0$ in Eq. (2)
3. ATI proliferation and non-linear direct self feedback or constant recruitment with linear direct self feedback: $r_A A - \frac{r_A}{K_A} A^2$ or $r_A - \frac{r_A}{K_A} A$ in Eq. (3).

Altogether, there are eight total models spanned by all the choices listed above, leading to seven alternate models to our original set of equations in Eqs. (1)–(3). With the same parameters examined for the original model (Table 1), we find that the bifurcation behavior remains qualitatively similar for all of the eight models (Fig. 5). However, there are several noticeable differences with the alternate models. One of these differences is that for each model except for the original, there is no stable, feasible **TP** state for any ω value. Additionally, when ATI dynamics are altered so that ATI cells are recruited in an A-independent manner and die at a constant rate, there is no **T** state, so that the tumor density of the **TPA** state, when it exists, is an increasing function of ω. For a more detailed analysis of the alternate models, see Appendices B & C.

When PTI cells have a non-linear self-limitation term, the saddle node bifurcation leading to bistability occurs at a lower ω value (Fig. 5). This difference is likely due to the fact that the value of P in the **TPA** state for the parameters we used is less than one, leading to less self-limitation than would occur with a linear self-limitation term. Thus, the saddle node bifurcation will likely occur at a larger ω value for these models than for those with linear PTI self-limitation terms with the same parameters.

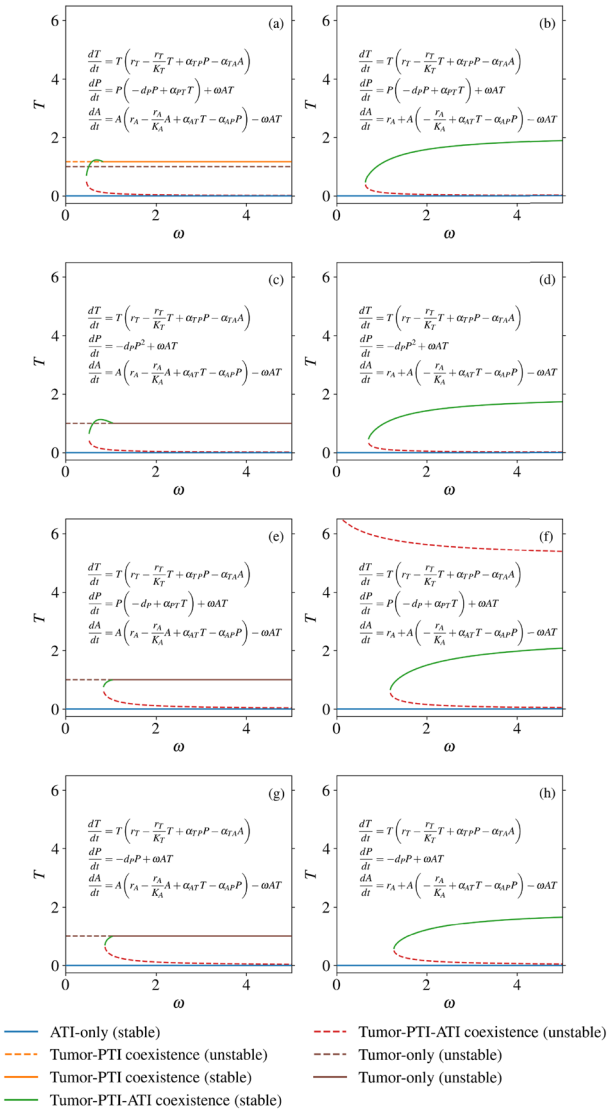

Fig. 5 Bifurcation diagrams showing the steady state density of tumor cells from all eight choices of model. **a** The model from Eqs. (1)–(3), analyzed in the above sections. **b** The model in (**a**) except with an ATI source term (immune cell recruitment) and a linear ATI death term. **c** The model in (**a**) without a PTI growth term dependent on tumor cells (equivalent to $\alpha_{PT} = 0$). **d** The model in (**c**) with an ATI source term and a linear ATI death term. **e** The model in (**a**) with a linear PTI death term. **f** The model in (**d**) with an ATI source term and a linear ATI death term. **g** The The model in (**a**) without a PTI growth term dependent on tumor cells and with a linear PTI death term. **h** The model in (**g**) with an ATI source term and a linear ATI death term. With a linear intrinsic ATI birth term and non-linear ATI death rate, in subplots (**a**), (**c**), (**e**), and (**g**), the stable tumor-PTI-ATI steady state collides either with the tumor-PTI coexistence state in (**a**) or with the tumor-only state in (**c**), (**e**), and (**g**). On the other hand, with an ATI source term and a linear ATI death term, in subplots (**b**), (**d**), (**f**), and (**h**), the stable tumor-PTI-ATI steady state does not collide with another steady state but saturates as ω increases (Color figure online)

4 Conclusions

We have analyzed the effects of tumor-induced immune cell conversion in a simple model of the TIME, finding that an immune cell conversion term allows for bistability between a cancer-free state and a state with a non-zero tumor cell density. Our results suggest an important role for immune cell conversion in the early stages of tumor growth, before the TIME has been shaped into a pro-tumor state, which in the context of our model is characterized by parameters for which there is no stable steady state with positive tumor density for $\omega = 0$. For a large enough immune cell conversion rate, we find that a "stalemate" or "equilibrium" stable steady state can exist. In this stalemate state, tumor cells, PTI cells, and ATI cells can coexist, maintained by a balance of pro-tumor and anti-tumor factors. Eventual escape from equilibrium tumor states, leading to tumor growth not limited by the anti-tumor immune system, is not directly captured by our model; perhaps including a direct competition for metabolic resources might allow a large enough tumor to completely suppress immunity. Instead, escape from a coexistence state can be caused by changes in model parameters so that a shift from a coexistence state to a stable tumor and PTI cell steady state occurs.

By assuming a quadratic form for ATI-induced tumor cell death ($-\alpha_{TA} T A$ in Eq. 1), we ignore the possibility of tumor cell population size-dependent or tumor growth rate-dependent immunosurveillance (Finn 2018). In the case where small tumor cell populations are not detected and/or targeted by the immune system, it is conceivable that a large enough tumor cell population can grow before ATI-induced tumor cell death becomes appreciable, allowing tumors to bypass the basin of attraction for **A** states when there is bistability with steady states characterized by a non-zero tumor cell density. In this case, the tumor cell population density at which the immune system begins killing tumor cells can be considered the initial state of a tumor in our model, and larger ATI-to-PTI conversion rates will place this initial state closer to the basin of attraction of cancer states. At the same time, our model suggests that an immune system able to successfully reduce a large tumor cell density may be able to bring tumor cell density to a threshold value, below which tumor clearance is nearly inevitable.

Previous work has suggested that tumor cell populations may subject to an Allee effect (Korolev et al. 2014; Böttger et al. 2015; Johnson et al. 2019; Azimzade et al. 2021). Allee effects can be classified as weak, where below a threshold population size the growth rate is non-negative but small, or strong, where below a threshold the growth rate is negative, driving the mean population size to zero. One suggested mechanism for an Allee effect in tumor population dynamics is cell-density dependence of "go or grow" phenotype switching (Böttger et al. 2015). Our ecological model of the TIME suggests that tumor-immune interactions, namely immune cell conversion, may also contribute to an Allee effect. Clearly, if a threshold initial population of tumor cells is necessary for the tumor to persist (on average), there is a significant barrier to tumor viability. As the ability of tumor cells to convert ATI cells to PTI cells increases, the threshold population size decreases, lowering the barrier for tumor viability as a function of initial population size.

Further work is needed to uncover the role of tumor-induced immune cell conversion on cancer dynamics. From the theoretical side, more realistic treatment of the immune system, together with consideration for the effects of spatial organization on

tumor growth and immune interaction could be incorporated into modeling efforts. In addition, phenotypic switching of tumor cells should be taken into account, especially since processes such as EMT might alter a cell's sensitivity to immune interdiction (Tripathi et al. 2016). Ideally, a quantitatively predictive model could be developed to allow for direct comparison with experiments, in order to test our theory-generated hypotheses concerning the role of immune cell conversion in tumor dynamics. Further, such a model could inform immunotherapy strategies targeting immune cell conversion, including attempts to promote M1 tumor-associated macrophage phenotypes over M2 phenotypes (Zhang et al. 2019; Li et al. 2020; Jaynes et al. 2020; Guo et al. 2023) and the targeting of regulatory T-cells (Tanaka and Sakaguchi 2019).

Acknowledgements This work was supported in part by the Center for Theoretical Biological Physics, NSF PHY-2019745.

Funding Open access funding provided by Northeastern University Library

Data Availability Code needed to produce all results and figures from this article is available at: https://github.com/amoffett/tumor-immune_ecology_2023.

Declarations

Conflict of interest The authors declare that they have no conflict of interest.

Appendix A Analysis of Steady States

A.1 Tumor-Only (T)

The tumor-only steady state (**T**) is

$$T = K_T, \;\; P = 0, \;\; A = 0 \tag{19}$$

and is always feasible in the allowed parameter space. The eigenvalues of the Jacobian for **T** are

$$\lambda \in \{-r_T, \;\; \alpha_{PT} K_T, \;\; r_A + (\alpha_{AT} - \omega) K_T\}, \tag{20}$$

so that the tumor-only steady state is always unstable because $\alpha_{PT} K_T > 0$.

A.2 ATI-Only (A)

The ATI-only steady state (**A**) is

$$T = 0,\ P = 0,\ A = K_A \tag{21}$$

with eigenvalues of the Jacobian

$$\lambda \in \{r_T - \alpha_{TA} K_A,\ 0,\ -r_A\}. \tag{22}$$

Because one of the eigenvalues is zero, we cannot conclude that **A** is stable under any conditions from linear stability analysis alone. However, a necessary condition for the the ATI-only steady state to be stable is

$$r_T < \alpha_{TA} K_A. \tag{23}$$

This means that for the cancer-free ATI-only state to be stable, the ability of ATI cells to reduce the growth rate of tumor cells at the maximal ATI population size (in the absence of other cell types) must outpace the intrinsic growth rate of tumor cells. We provide numerical evidence that **A** is stable when Eq. (23) is satisfied, by numerically integrating Eqs. (1)–(3) for 5000 randomly chosen, feasible initial conditions sampled from an open ball with radius 0.1 around the **A** steady state (Fig. 6). See Table 1 for parameters used in Fig. 6. When $\alpha_{AT} = 1$, we have $r_T = \alpha_{TA} K_A$ (for $r_T = K_A = 1$) and we do not necessarily expect **A** to be stable. While **A** appears to be stable for $\omega = 0$ in this case, for all other chosen ω values **A** is not stable; the final state of almost every single trajectory is further away from **A** than the initial state and appears to converge to a different steady state. On the other hand, for $\alpha_{TA} = 1.25$ and $\alpha_{TA} = 1.5$, for all ω values, there is an open ball around **A** within which each trajectory moves towards **A**. This suggests that **A** is stable for these two parameter sets with $r_T < \alpha_{TA} K_A$. Invoking our definition of the invasion growth rate in Eq. (12), we can rewrite the condition in Eq. (23) by defining the invasibility of a healthy system (meaning in the ATI-only state) by tumor cells as

$$\Omega_{T\to\mathbf{A}} \equiv \lim_{T\to 0^+} \frac{1}{T}\frac{dT}{dt}\bigg|_{\mathbf{N}=\mathbf{A}+\delta\mathbf{N}} = r_T - \alpha_{TA} K_A \tag{24}$$

with

$$\delta\mathbf{N} = \begin{bmatrix} T \\ 0 \\ 0 \end{bmatrix}. \tag{25}$$

When $\Omega_{T\to\mathbf{A}} > 0$, tumor cells can invade and when $\Omega_{T\to\mathbf{A}} \leq 0$ they cannot. We can restate the stability condition in Eq. (23) in terms of tumor invasibility as

$$\Omega_{T\to\mathbf{A}} < 0. \tag{26}$$

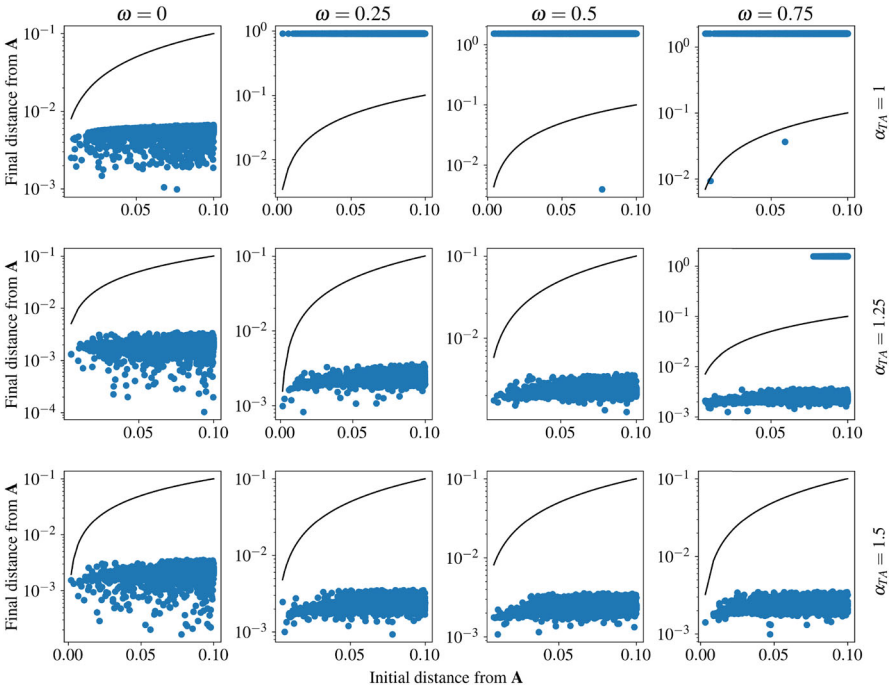

Fig. 6 Numerical integration of Eqs. (1)–(3) for small perturbations around the **A** state. The first row uses $\alpha_{TA} = 1$, the second $\alpha_{TA} = 1.25$, and the third $\alpha_{TA} = 1.5$. The columns use $\omega = 0$, 0.25, 0.5 and 0.75. Each subplot shows the initial distance from the **A** state on the x-axis and the final distance after integration over 500 time units for 5,000 randomly chosen initial conditions. Initial conditions were sampled from the open ball with radius 0.1 around the **A** state, and chosen so that they were all feasible. The black line in each subplot shows the line $y = x$ (Colour figure online)

A.3 Tumor-ATI Coexistence (TA)

The tumor-ATI steady state (**TA**) can only exist when $\omega = 0$, because otherwise the combination of tumor cells and ATI cells would produce PTI cells, adding PTI cell density. Setting Eqs. (1)–(3) equal to zero, and substituting $P = 0$ and $\omega = 0$, we have the following equations

$$0 = r_T - \frac{r_T}{K_T} T - \alpha_{TA} A \tag{27}$$

$$0 = r_A - \frac{r_A}{K_A} A + \alpha_{AT} T \tag{28}$$

which we can solve and rearrange to find the **TA** state

$$T = K_T \left(1 - \frac{\alpha_{TA}}{r_T} \frac{\Omega_{A \to \mathbf{T}}}{\Gamma_{A \to A;\mathbf{TA}}}\right) \tag{29}$$

$$P = 0 \tag{30}$$

$$A = \frac{\Omega_{A\to\mathbf{T}}}{\Gamma_{A\to A;\mathbf{TA}}}. \tag{31}$$

The invasibility of the tumor-only state by ATI cells and the net negative feedback of ATI cells on themselves in the tumor-ATI coexistence steady state are defined as

$$\Omega_{A\to\mathbf{T}} = r_A + \alpha_{AT} K_T \tag{32}$$

$$\Gamma_{A\to A;\mathbf{TA}} = \frac{r_A}{K_A} + \frac{\alpha_{AT}\alpha_{TA}}{r_T/K_T}, \tag{33}$$

respectively. Both quantities arise in the solution of Eqs. (27) and (28), and $\Omega_{A\to\mathbf{T}}$ (Eq. 32) can be defined in a similar way to $\Omega_{T\to\mathbf{A}}$ (Eq. 24). In contrast to the case of tumor cells invading the **A** state, tumor cell density has a positive effect of the growth rate of ATI cells, so that $\Omega_{A\to\mathbf{T}}$ increases with the tumor carrying capacity, K_T. Note that both $\Omega_{A\to\mathbf{T}}$ and $\Gamma_{A\to A;\mathbf{TA}}$ are non-negative, so that the tumor-ATI coexistence steady state is feasible when

$$r_T - \alpha_{TA}\frac{\Omega_{A\to\mathbf{T}}}{\Gamma_{A\to A;\mathbf{TA}}} > 0. \tag{34}$$

This condition can be interpreted to mean that the tumor-ATI coexistence steady state is feasible when the growth of the tumor outpaces tumor death due to ATI cells. The tumor-ATI coexistence state is unstable, as when a small density of PTI ($\delta P > 0$) is added to the system, the net growth rate of PTI cells (plugging δP into Eq. (2) with $\omega = 0$)

$$\frac{dP}{dt} = \alpha_{PT} T \delta P - d_P \delta P^2 \tag{35}$$

will be positive. It is clear that when

$$\delta P < \frac{\alpha_{PT} T}{d_P} \tag{36}$$

is satisfied Eq. (35) is positive, providing an explicit definition for a "small density" in this case.

A.4 Tumor-PTI Coexistence (TP)

We can find the tumor-PTI coexistence steady state (**TP**) by again setting Eqs. (1)–(3) equal to zero, and substituting $A = 0$ to yield

$$0 = r_T - \frac{r_T}{K_T} T + \alpha_{TP} P \tag{37}$$

$$0 = -d_P P + \alpha_{PT} T \tag{38}$$

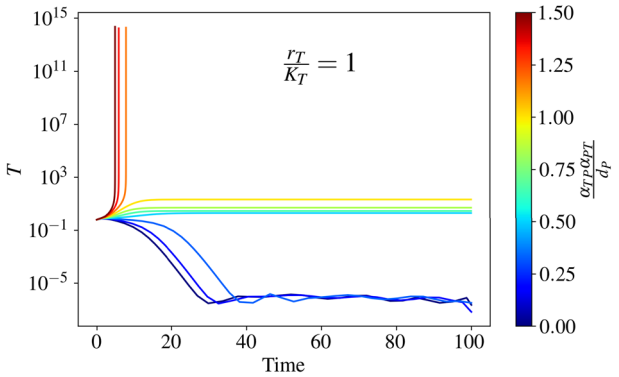

Fig. 7 Numerical integration of Eqs. (1)–(3), showing unbounded growth of tumor cell density when $\frac{\alpha_{TP}\alpha_{PT}}{d_P} \geq \frac{r_T}{K_T}$. We varied α_{PT} while keeping α_{TP} and d_P fixed (Colour figure online)

which we can solve for

$$T = \frac{r_T}{\Gamma_{T\to T;\mathbf{TP}}} \tag{39}$$

$$P = \frac{\alpha_{PT}}{d_P}\frac{r_T}{\Gamma_{T\to T;\mathbf{TP}}} \tag{40}$$

$$A = 0. \tag{41}$$

The net negative feedback of tumor cells on themselves in this steady state is defined as

$$\Gamma_{T\to T;\mathbf{TP}} = \frac{r_T}{K_T} - \frac{\alpha_{TP}\alpha_{PT}}{d_P} \tag{42}$$

which, as for the **TA** solution, arises from rearranging the **TP** solution. In order for tumor-PTI coexistence to be feasible, the negative feedback of tumor cells on themselves must be positive,

$$\Gamma_{T\to T;\mathbf{TP}} > 0, \tag{43}$$

meaning that the direct, negative feedback of tumor cells on themselves (r_T/K_T) must exceed, in magnitude, the positive feedback of tumor cells on themselves through PTI cells ($\frac{\alpha_{TP}\alpha_{PT}}{d_P}$). When $\Gamma_{T\to T;\mathbf{TP}} \leq 0$, we observe in numerical integration of Eqs. (1)–(3) that the tumor density can grow in an apparently unbounded manner (Fig. 7).

Unlike for previously discussed steady states, the stability of the tumor-PTI coexistence steady state is dependent on the ATI-to-PTI conversion rate ω. The eigenvalues of the Jacobian are

$$\lambda \in \left\{ r_A + \frac{r_T}{\Gamma_{T\to T;\mathbf{TP}}}\left(\alpha_{AT} - \omega - \frac{\alpha_{AP}\alpha_{PT}}{d_P}\right), \right. \tag{44}$$

$$- \frac{r_T}{2\Gamma_{T\to T;\mathbf{TP}}}\left(\frac{r_T}{K_T} + \alpha_{PT} + \sqrt{\left(\frac{r_T}{K_T} - \alpha_{PT}\right)^2 + 4\frac{\alpha_{TP}\alpha_{PT}^2}{d_P}}\right), \tag{45}$$

$$- \frac{r_T}{2\Gamma_{T\to T;\mathbf{TP}}}\left(\frac{r_T}{K_T} + \alpha_{PT} - \sqrt{\left(\frac{r_T}{K_T} - \alpha_{PT}\right)^2 + 4\frac{\alpha_{TP}\alpha_{PT}^2}{d_P}}\right)\Bigg\} \tag{46}$$

As long as

$$\omega > \Gamma_{T\to T;\mathbf{TP}}\frac{r_A}{r_T} + \alpha_{AT} - \frac{\alpha_{AP}\alpha_{PT}}{d_P} \tag{47}$$

holds then the first eigenvalue (Eq. 44) will be negative. The second eigenvalue (Eq. 45) will always be negative, while the third eigenvalue (Eq. 46) be negative only when the condition

$$\frac{r_T}{K_T} > \frac{\alpha_{TP}\alpha_{PT}}{d_P} \tag{48}$$

is met. However, this condition is identical to that required for feasibility of the tumor-PTI coexistence state (Eq. 43). Thus, when the tumor-PTI coexistence state is feasible, it is stable if and only if the condition in Eq. (47) is met. When the right-hand side of Eq. (47) is negative, the tumor-PTI coexistence steady state is stable for all $\omega \geq 0$, provided that Eq. (48) is also satisfied. We can write the condition of right-hand side of Eq. (47) being negative as

$$0 > r_A - \Gamma_{T\to A;\mathbf{TP}}\frac{r_T}{\Gamma_{T\to T;\mathbf{TP}}} \tag{49}$$

with

$$\Gamma_{T\to A;\mathbf{TP}} = \frac{\alpha_{AP}\alpha_{PT}}{d_P} - \alpha_{AT}. \tag{50}$$

This corresponds to the invasion growth rate of ATI cells in the **TP** steady state, so that if ATI cells cannot invade then **TP** is stable for all $\omega \geq 0$. Accordingly, we can write the condition in Eq. (49) as

$$\Omega_{A\to\mathbf{TP}} < 0 \tag{51}$$

with

$$\begin{aligned}\Omega_{A\to\mathbf{TP}} &= r_A - \Gamma_{T\to A;\mathbf{TP}}\frac{r_T}{\Gamma_{T\to T;\mathbf{TP}}} \\ &= r_A - \alpha_{AP}\frac{\alpha_{PT}}{d_P}\frac{r_T}{\Gamma_{T\to T;\mathbf{TP}}} + \alpha_{AT}\frac{r_T}{\Gamma_{T\to T;\mathbf{TP}}}.\end{aligned} \tag{52}$$

Comparing with the steady state values of T and P in Eqs. (39) and (40), we can see the influence of both steady state tumor cell density and PTI cell density on the ATI cell invasion growth rate $\Omega_{A\to\mathbf{TP}}$.

A.5 Tumor-PTI-ATI Coexistence (TPA) Without PTI to ATI Conversion ($\omega = 0$)

When $\omega = 0$, the tumor-PTI-ATI (**TPA**) coexistence steady state can be solved for from a system of linear equations, as we solved for the **TA** and **TP** states. Once again, we set Eqs. (1)–(3) equal to zero, and set $\omega = 0$ to yield

$$0 = r_T - \frac{r_T}{K_T} T + \alpha_{TP} P \tag{53}$$

$$0 = -d_P P + \alpha_{PT} T \tag{54}$$

$$0 = r_A - \frac{r_A}{K_A} A + \alpha_{AT} T - \alpha_{AP} P. \tag{55}$$

Solving for T, P, and A and rearranging terms, we have

$$T = \frac{\Omega_{T\to\mathbf{A}}}{\Gamma_{T\to T;\mathbf{TPA}}} \tag{56}$$

$$P = \frac{\alpha_{PT}}{d_P} \frac{\Omega_{T\to\mathbf{A}}}{\Gamma_{T\to T;\mathbf{TPA}}} \tag{57}$$

$$A = K_A - \frac{\Gamma_{T\to A;\mathbf{TPA}}}{r_A/K_A} \frac{\Omega_{T\to\mathbf{A}}}{\Gamma_{T\to T;\mathbf{TPA}}}. \tag{58}$$

where the net negative feedback with zero ATI to PTI conversion from tumor cells on themselves and on ATI cells, respectively, is

$$\Gamma_{T\to T;\mathbf{TPA}} = \frac{r_T}{K_T} + \frac{\alpha_{TA}\alpha_{AT}}{r_A/K_A} - \frac{\alpha_{TA}\alpha_{AP}\alpha_{PT}}{(r_A/K_A)d_P} - \frac{\alpha_{TP}\alpha_{PT}}{d_P} \tag{59}$$

$$\Gamma_{T\to A;\mathbf{TPA}} = \frac{\alpha_{AP}\alpha_{PT}}{d_P} - \alpha_{AT} \tag{60}$$

and $\Omega_{T\to\mathbf{A}}$ is defined as in Eq. (24). Note that $-\alpha_{PT}$ can similarly be defined as the net negative tumor to PTI feedback.

Clearly, a necessary condition for the tumor-PTI-ATI coexistence steady state to be feasible is that the signs of $\Omega_{T\to\mathbf{A}}$ and $\Gamma_{T\to T;\mathbf{TPA}}$ must be the same. If we perturb the steady state when $\Gamma_{T\to T;\mathbf{TPA}} < 0$, however, we can see that it is unstable. For a small, positive perturbation of the tumor cell density ($\delta T > 0$), we define the overall perturbation

$$\delta\mathbf{N} = \begin{bmatrix} \delta T \\ \frac{\alpha_{PT}}{d_P}\delta T \\ -\frac{\Gamma_{T\to A;\mathbf{TPA}}}{r_A/K_A}\delta T \end{bmatrix} \tag{61}$$

and then plug this into Eq. (1) for the change in tumor cell density, with T, P, and A taking on the values in Eqs. (56)–(58), to find

$$\frac{dT}{dt} = (T + \delta T)\left(r_T - \frac{r_T}{K_T}(T + \delta T) + \alpha_{TP}\left(P + \frac{\alpha_{PT}}{d_P}\delta T\right)\right.$$

$$
\begin{aligned}
&- \alpha_{TA}\left(A - \frac{\Gamma_{T\to A;\mathbf{TPA}}}{K_A/r_A}\delta T\right)\Bigg) \\
&= (T+\delta T)\left(-\frac{r_T}{K_T}\delta T + \frac{\alpha_{TP}\alpha_{PT}}{d_P}\delta T + \frac{\alpha_{TA}\Gamma_{T\to A;\mathbf{TPA}}}{K_A/r_A}\delta T\right) \\
&= -\Gamma_{T\to T;\mathbf{TPA}}(T+\delta T)\delta T. \qquad (62)
\end{aligned}
$$

If $\Gamma_{T\to T;\mathbf{TPA}} < 0$, as we have assumed, then the tumor cell density will increase, failing to restore the system to the steady state. Checking for P

$$
\begin{aligned}
\frac{dP}{dt} &= \left(P + \frac{\alpha_{PT}}{d_P}\delta T\right)\left(-d_P\left(P + \frac{\alpha_{PT}}{d_P}\delta T\right) + \alpha_{PT}(T+\delta T)\right) \\
&= \left(P + \frac{\alpha_{PT}}{d_P}\delta T\right)(\alpha_{PT}\delta T - \alpha_{PT}\delta T) = 0 \qquad (63)
\end{aligned}
$$

and A

$$
\begin{aligned}
\frac{dA}{dt} &= \left(A - \frac{\Gamma_{T\to A;\mathbf{TPA}}}{r_A/K_A}\delta T\right)\left(r_A - \frac{r_A}{K_A}\left(A - \frac{\Gamma_{T\to A;\mathbf{TPA}}}{r_A/K_A}\delta T\right)\right. \\
&\quad \left. + \alpha_{AT}(T+\delta T) - \alpha_{AP}\left(P + \frac{\alpha_{PT}}{d_P}\delta T\right)\right) \\
&= \left(A - \frac{\Gamma_{T\to A;\mathbf{TPA}}}{r_A/K_A}\delta T\right)\left(\Gamma_{T\to A;\mathbf{TPA}}\delta T + \alpha_{AT}\delta T - \frac{\alpha_{AP}\alpha_{PT}}{d_P}\delta T\right) = 0 \qquad (64)
\end{aligned}
$$

we see that both the PTI and ATI density remain unchanged, so that the system moves away from the tumor-PTI-ATI coexistence steady state. The stability of the steady state when $\Gamma_{T\to T;\mathbf{TPA}} > 0$ can be checked for each specific case by examining the eigenvalues of the Jacobian matrix, as before.

A.6 Tumor-PTI-ATI Coexistence (TPA) with PTI to ATI Conversion ($\omega \geq 0$)

We now examine the full steady-state behavior of the model as the ATI to PTI conversion rate is varied. Rearranging the nullclines (setting each of Eqs. (1)–(3) to zero) for steady states in $\mathcal{S}_{\mathbf{TPA}}$, we find the system of equations

$$
\begin{aligned}
T &= K_T + \frac{\alpha_{TP}K_T}{r_T}P - \frac{\alpha_{TA}K_T}{r_T}A \qquad (65)\\
T &= \frac{d_P P^2}{\alpha_{PT}P + \omega A} \qquad (66)\\
T &= -\frac{r_A}{\alpha_{AT}-\omega} + \frac{\alpha_{AP}}{\alpha_{AT}-\omega}P + \frac{r_A}{K_A(\alpha_{AT}-\omega)}A. \qquad (67)
\end{aligned}
$$

In order to find the steady state, we find the intersection of the two planes (Eqs. 65 and 67) in terms of P

$$A_{P,\omega} = \frac{r_A(r_T/K_T) + r_T(\alpha_{AT} - \omega)}{(r_A/K_A)(r_T/K_T) + \alpha_{TA}(\alpha_{AT} - \omega)} - \frac{\alpha_{AP}(r_T/K_T) - \alpha_{TP}(\alpha_{AT} - \omega)}{(r_A/K_A)(r_T/K_T) + \alpha_{TA}(\alpha_{AT} - \omega)} P \tag{68}$$

and then look for intersections with Eq. (66) using Eqs. (65) and (68)

$$K_T + \frac{\alpha_{TP} K_T}{r_T} P - \frac{\alpha_{TA} K_T}{r_T} A_{P,\omega} = \frac{d_P P^2}{\alpha_{PT} P + \omega A_{P,\omega}}. \tag{69}$$

Rearranging Eq. (69) into the form

$$aP^2 + bP + c = 0, \tag{70}$$

we can easily solve for P, and subsequently find T and A. The bifurcation diagrams in Fig. 2 illustrate the behavior of all the steady states (except for the tumor-only steady state) as ω is varied, for parameters where all the steady states of interest are feasible. When $r_T - \alpha_{TA} K_A = 0$ (first row of Fig. 2), the tumor density is zero at steady state at $\omega = 0$. For all $\omega > 0$, the system is bistable, with the tumor density either at zero, or for the tumor-PTI-ATI coexistence state, at a positive number. The steady state with non-zero tumor density continuously increases until ω reaches $\Gamma_{T\to T;\mathbf{TP}} \frac{r_A}{r_T} + \alpha_{AT} - \frac{\alpha_{AP}\alpha_{PT}}{d_P}$ (Eq. 47), when the tumor-PTI-ATI coexistence solution and the tumor-PTI coexistence solution collide, resulting in a transcritical bifurcation (note that we only depict feasible states in Fig. 2). As the rate of tumor death due to ATI cells (α_{TA}) increases, we can see that a saddle node bifurcation gives rise to a stable and an unstable tumor-PTI coexistence solution at a positive ω. The ω value where this saddle node bifurcation occurs increases with α_{TA}, meaning that tumors need to convert ATI cells to PTI cells at a higher rate in order for a stable tumor population to exist as ATI cells kill tumor cells more rapidly.

When α_{TA} is large enough, the value of ω for which the saddle node bifurcation occurs reaches the value of ω for which the tumor-PTI-ATI and tumor-PTI solution collide (Fig. 3). When these two values of ω coincide, there is no longer a saddle node bifurcation creating the two tumor-PTI-ATI solutions, but rather a subcritical pitchfork bifurcation giving rise to two unstable tumor-PTI-ATI solutions. At higher α_{TA} values, the saddle node bifurcation reappears, but now the branch with lower tumor density has a stable region, which is infeasible.

Appendix B Alternate Models: Modifications to PTI Dynamics

There are several reasonable changes one could make to the model presented in the main text,

$$\frac{dT}{dt} = T\left(r_T - \frac{r_T}{K_T} T + \alpha_{TP} P - \alpha_{TA} A\right) \tag{71}$$

$$\frac{dP}{dt} = P\left(-d_P P + \alpha_{PT} T \right) + \omega AT \tag{72}$$

$$\frac{dA}{dt} = A\left(r_A - \frac{r_A}{K_A} A + \alpha_{AT} T - \alpha_{AP} P \right) - \omega AT. \tag{73}$$

The alternate models we consider involve changes to the PTI dynamics, in this Appendix, and to the ATI dynamics, in Appendix C.

A.7 Linear PTI Death Rate

For the changes to the PTI dynamics, we first consider the consequences of changing the PTI death rate to be linear

$$\frac{dP}{dt} = P\left(-d_P + \alpha_{PT} T \right) + \omega AT. \tag{74}$$

For this model, there can be **T**, **A**, **TA**, and **TP** steady states and up to two **TPA** steady states. The actual **T**, **A**, and **TA** state vectors are the same as in the original model. The stability of **T** can switch as ω is changed, due to a transcritical bifurcation resulting from a collision with a stable **TPA** state. The conditions for **T** stability are

$$d_P > \alpha_{PT} K_T \tag{75}$$

$$\omega > \alpha_{AT} + \frac{r_A}{K_T}. \tag{76}$$

The **A** steady state has the exact same stability conditions as in the original model, while **TA**, which is equal to **TA** in the original model and can still only exist when $\omega = 0$, can now be stable if $d_P > \alpha_{PT} K_T \left(1 - \frac{\alpha_{TA}}{r_T} \frac{\Omega_{A\to\mathbf{T}}}{\Gamma_{A\to A;\mathbf{TA}}}\right)$. The **TP** state can exist in this alternate model with densities

$$T = \frac{d_P}{\alpha_{PT}} \tag{77}$$

$$P = \frac{r_T (d_P - \alpha_{PT} K_T)}{K_T \alpha_{PT} \alpha_{TP}} \tag{78}$$

$$A = 0 \tag{79}$$

and stability conditions

$$d_P < \alpha_{PT} K_T \tag{80}$$

$$\omega > \alpha_{AT} + \frac{r_A \alpha_{PT}}{d_P} - \frac{\alpha_{AP} r_T (d_P - K_T \alpha_{PT})}{d_P \alpha_{TP}}. \tag{81}$$

Note that the PTI density of **TP** can only be positive when the first stability condition is not met (that is, when $d_P > \alpha_{PT} K_T$). Thus, when **TP** is feasible, it is unstable.

To find the **TPA** states, we can use the approach described for the original model, substituting

$$T = \frac{d_P P}{\alpha_{PT} P + \omega A} \tag{82}$$

for Eq. 66. This again leads to a quadratic equation in P, from which we can solve for two **TPA** steady states.

A.8 No ATI-Independent Effect of Tumor Density of PTI Dynamics

Next, we analyze an alternate model where the PTI death rate is nonlinear, but there is ATI-independent effect of tumor density of PTI dynamics ($\alpha_{PT} = 0$)

$$\frac{dP}{dt} = -d_P P^2 + \omega A T. \tag{83}$$

Here, there can be **T**, **A**, and **TA** steady states and up to two **TPA** steady states. The actual **T**, **A**, and **TA** state vectors are again the same as in the original model. The **T** state has the single stability condition

$$\omega > \alpha_{AT} + \frac{r_A}{K_T} \tag{84}$$

while the **A** state has the same stability criteria as in the previous section. Again, for the **TPA** states, we can use the approach described for the original model, substituting

$$T = \frac{d_P P^2}{\omega A} \tag{85}$$

for Eq. (66), yielding a quadratic equation in P and up to two **TPA** steady states.

A.9 Linear PTI Death Rate and No ATI-Independent Effect of Tumor Density of PTI Dynamics

Finally, we can make both changes to the PTI dynamics simultaneously, yielding

$$\frac{dP}{dt} = -d_P P + \omega A T. \tag{86}$$

This model yields similar results as in Appendix A.8, except that to find the **TPA** states, we substitute

$$T = \frac{d_P P}{\omega A} \tag{87}$$

for Eq. (66) and solve the quadratic equation for P, yielding up to two **TPA** steady states.

Appendix C Alternate Models: Modifications to ATI Dynamics

The final modification to our original model that we examine is to the ATI dynamics, where now ATI cells are recruited at a constant rate and die at a constant rate, yielding

$$\frac{dA}{dt} = r_A + A\left(- \frac{r_A}{K_A} + \alpha_{AT} T - \alpha_{AP} P \right) - \omega A T. \tag{88}$$

There are now no **T** and **TP** states, because of ATI recruitment (r_A). The **A** state and its stability condition are exactly the same as in all other models.

Looking at the nullclines of the model, with each of the four possible models for PTI dynamics, we have

$$T = K_T + \frac{\alpha_{TP} K_T}{r_T} P - \frac{\alpha_{TA} K_T}{r_T} A \tag{89}$$

$$T = \frac{d_P P^2}{\alpha_{PT} P + \omega A} \text{ or } T = \frac{d_P P}{\alpha_{PT} P + \omega A} \text{ or } T = \frac{d_P P^2}{\omega A} \text{ or } T = \frac{d_P P}{\omega A} \tag{90}$$

$$T = \frac{r_A}{K_A(\alpha_{AT} - \omega)} + \frac{\alpha_{AP}}{\alpha_{AT} - \omega} P - \frac{r_A}{(\alpha_{AT} - \omega)} A^{-1} \tag{91}$$

from which we can solve for P in terms of A

$$P_{A,\omega} = \left(\frac{\alpha_{AP}}{\alpha_{AT} - \omega} - \frac{\alpha_{TP} K_T}{r_T} \right)^{-1} \left(K_T - \frac{r_A}{K_A(\alpha_{AT} - \omega)} - \frac{\alpha_{TA} K_T}{r_T} A + \frac{r_A}{(\alpha_{AT} - \omega)} A^{-1} \right). \tag{92}$$

Choosing, for example, the original PTI model dynamics, we end up with the equation

$$K_T + \frac{\alpha_{TP} K_T}{r_T} P_{A,\omega} - \frac{\alpha_{TA} K_T}{r_T} A = \frac{d_P P_{A,\omega}^2}{\alpha_{PT} P_{A,\omega} + \omega A} \tag{93}$$

This leads to a degree four polynomial, with at most four roots. The solutions for A can then be used to find the **TPA** states.

References

Aktipis CA, Boddy AM, Jansen G et al (2015) Cancer across the tree of life: cooperation and cheating in multicellularity. Philos Trans R Soc B Biol Sci 370(1673):20140219

Anderson NM, Simon MC (2020) The tumor microenvironment. Curr Biol 30(16):R921–R925

Arabameri A, Asemani D, Hadjati J (2018) A structural methodology for modeling immune-tumor interactions including pro-and anti-tumor factors for clinical applications. Math Biosci 304:48–61

Azimzade Y, Saberi AA, Gatenby RA (2021) Superlinear growth reveals the allee effect in tumors. Phys Rev E 103(4):042405

Ben-Jacob E, Coffey DS, Levine H (2012) Bacterial survival strategies suggest rethinking cancer cooperativity. Trends Microbiol 20(9):403–410

Binnewies M, Roberts EW, Kersten K et al (2018) Understanding the tumor immune microenvironment (time) for effective therapy. Nat Med 24(5):541–550
Biswas SK, Mantovani A (2010) Macrophage plasticity and interaction with lymphocyte subsets: cancer as a paradigm. Nat Immunol 11(10):889–896
Böttger K, Hatzikirou H, Voss-Böhme A et al (2015) An emerging allee effect is critical for tumor initiation and persistence. PLoS Comput Biol 11(9):e1004366
Bunin G (2017) Ecological communities with Lotka-Volterra dynamics. Phys Rev E 95(4):042414
De Visser KE, Eichten A, Coussens LM (2006) Paradoxical roles of the immune system during cancer development. Nat Rev Cancer 6(1):24–37
Eftimie R, Hamam H (2017) Modelling and investigation of the cd4+ t cells-macrophages paradox in melanoma immunotherapies. J Theor Biol 420:82–104
Finn OJ (2018) A believer's overview of cancer immunosurveillance and immunotherapy. J Immunol 200(2):385–391
Flavell RA, Sanjabi S, Wrzesinski SH et al (2010) The polarization of immune cells in the tumour environment by tgfβ. Nat Rev Immunol 10(8):554–567
Gao Y, Souza-Fonseca-Guimaraes F, Bald T et al (2017) Tumor immunoevasion by the conversion of effector nk cells into type 1 innate lymphoid cells. Nat Immunol 18(9):1004–1015
Gatenbee CD, Baker AM, Schenck RO et al (2022) Immunosuppressive niche engineering at the onset of human colorectal cancer. Nat Commun 13(1):1798
Gerlinger M, McGranahan N, Dewhurst SM et al (2014) Cancer: evolution within a lifetime. Annu Rev Genet 48(1):215–36
Gluzman M, Scott JG, Vladimirsky A (2020) Optimizing adaptive cancer therapy: dynamic programming and evolutionary game theory. Proc R Soc B 287(1925):20192454
Guo Y, Fan L, Wang X (2023) Mathematical investigation of the role of re-polarisation of m2 in cancer therapy. Discrete Contin Dyn Syst B 28(4):2718–2744
Hamilton PT, Anholt BR, Nelson BH (2022) Tumour immunotherapy: lessons from predator–prey theory. Nat Rev Immunol 22:765
Harris CR, Millman KJ, van der Walt SJ et al (2020) Array programming with NumPy. Nature 585(7825):357–362. https://doi.org/10.1038/s41586-020-2649-2
Hunter JD (2007) Matplotlib: a 2D graphics environment. Comput Sci Eng 9(3):90–95
Jaynes JM, Sable R, Ronzetti M et al (2020) Mannose receptor (cd206) activation in tumor-associated macrophages enhances adaptive and innate antitumor immune responses. Sci Transl Med 12(530):eaax6337
Jetten N, Verbruggen S, Gijbels MJ et al (2014) Anti-inflammatory m2, but not pro-inflammatory m1 macrophages promote angiogenesis in vivo. Angiogenesis 17:109–118
Johnson KE, Howard G, Mo W et al (2019) Cancer cell population growth kinetics at low densities deviate from the exponential growth model and suggest an allee effect. PLoS Biol 17(8):e3000399
Kareva I, Luddy KA, O'Farrelly C et al (2021) Predator-prey in tumor-immune interactions: A wrong model or just an incomplete one? Front. Immuno. 12:3391
Kessler DA, Levine H (2022) Phenomenological approach to cancer cell persistence. Phys Rev Lett 129(10):108101
Kluyver T, Ragan-Kelley B, Pérez F et al (2016) Jupyter notebooks - a publishing format for reproducible computational workflows. In: Loizides F, Schmidt B (eds) Positioning and power in academic publishing: players, agents and agendas. IOS Press, Amsterdam, pp 87–90
Koebel CM, Vermi W, Swann JB et al (2007) Adaptive immunity maintains occult cancer in an equilibrium state. Nature 450(7171):903–907
Korolev KS, Xavier JB, Gore J (2014) Turning ecology and evolution against cancer. Nat Rev Cancer 14(5):371–380
Li J, Zhao M, Sun M et al (2020) Multifunctional nanoparticles boost cancer immunotherapy based on modulating the immunosuppressive tumor microenvironment. ACS Appl Mater 12(45):50734–50747
Li X, Gruosso T, Zuo D et al (2019) Infiltration of cd8+ t cells into tumor cell clusters in triple-negative breast cancer. Proc Natl Acad Sci 116(9):3678–3687
Li X, Jolly MK, George JT et al (2019) Computational modeling of the crosstalk between macrophage polarization and tumor cell plasticity in the tumor microenvironment. Front Oncol 9:10
Liu VC, Wong LY, Jang T et al (2007) Tumor evasion of the immune system by converting cd4+ cd25- t cells into cd4+ cd25+ t regulatory cells: role of tumor-derived tgf-β. J Immunol 178(5):2883–2892

McFarland CD, Mirny LA, Korolev KS (2014) Tug-of-war between driver and passenger mutations in cancer and other adaptive processes. Proc Natl Acad Sci 111(42):15138–15143
Navin NE (2014) Cancer genomics: one cell at a time. Genome Biol 15(8):1–13
Nowell PC (1976) The clonal evolution of tumor cell populations: acquired genetic lability permits stepwise selection of variant sublines and underlies tumor progression. Science 194(4260):23–28
Pedregosa F, Varoquaux G, Gramfort A et al (2011) Scikit-learn: machine learning in Python. J Mach Learn Res 12:2825–2830
Reynolds BA, Oli MW, Oli MK (2020) Eco-oncology: applying ecological principles to understand and manage cancer. Ecol Evol 10(16):8538–8553
Roy DG, Kaymak I, Williams KS et al (2021) Immunometabolism in the tumor microenvironment. Ann Rev Cancer Biol 5:137–159
Schreiber RD, Old LJ, Smyth MJ (2011) Cancer immunoediting: integrating immunity's roles in cancer suppression and promotion. Science 331(6024):1565–1570
Shu Y, Huang J, Dong Y et al (2020) Mathematical modeling and bifurcation analysis of pro-and anti-tumor macrophages. Appl Math Model 88:758–773
Simeonov KP, Byrns CN, Clark ML et al (2021) Single-cell lineage tracing of metastatic cancer reveals selection of hybrid EMT states. Cancer Cell 39(8):1150–1162
Tanaka A, Sakaguchi S (2019) Targeting treg cells in cancer immunotherapy. Eur J Immunol 49(8):1140–1146
Tripathi SC, Peters HL, Taguchi A et al (2016) Immunoproteasome deficiency is a feature of non-small cell lung cancer with a mesenchymal phenotype and is associated with a poor outcome. Proc Natl Acad Sci 113(11):E1555–E1564
Virtanen P, Gommers R, Oliphant TE et al (2020) SciPy 1.0: fundamental algorithms for scientific computing in Python. Nat Methods 17:261–272. https://doi.org/10.1038/s41592-019-0686-2
Wang N, Liang H, Zen K (2014) Molecular mechanisms that influence the macrophage m1–m2 polarization balance. Front Immunol 5:614
Wangersky PJ (1978) Lotka-Volterra population models. Annu Rev Ecol Syst 9(1):189–218
Wilson S, Levy D (2012) A mathematical model of the enhancement of tumor vaccine efficacy by immunotherapy. Bull Math Biol 74(7):1485–1500
Wu CI, Wang HY, Ling S et al (2016) The ecology and evolution of cancer: the ultra-microevolutionary process. Annu Rev Genet 50:347–69
Zhang F, Parayath N, Ene C et al (2019) Genetic programming of macrophages to perform anti-tumor functions using targeted mrna nanocarriers. Nat Commun 10(1):3974